A Dual Quaternion Solution to Attitude and Position Control for Rigid-Body Coordination

Xiangke Wang, Changbin Yu, and Zhiyun Lin

***Abstract*—This paper focuses on finding a dual quaternion solution to attitude and position control for multiple rigid body coordination. Representing rigid bodies in 3-D space by unit dual quaternion kinematics, a distributed control strategy, together with a specified rooted-tree structure, are proposed to control the attitude and position of networked rigid bodies simultaneously with notion concision and nonsingularity. A property called *pairwise asymptotic stability* of the overall system is then analyzed and validated by an example of seven quad-rotor formation in the Urban Search And Rescue Simulation (USARSim) platform. As a separate but related issue, a maximum depth condition of the rooted tree is found with respect to error accumulation along each path using dual quaternion algebra, such that a given safety bound on attitude and position errors can be satisfied.**

***Index Terms*—Attitude and position, error accumulation, multiple rigid-body coordination, pairwise asymptotic stability (PAS), unit dual quaternion.**

I. Introduction

Multiagent systems have attracted significant research interest in recent years [1]–[6]. Nevertheless, little work has investigated cooperative agents within 3-D space with 6 degrees of freedom (DOFs) (including three rotational and three translational DOFs). Moving toward systems that are somewhat closer to certain practical applications in 3-D space, such as space-based interferometers, multiple spacecraft formation flying, multiple marine robotic explorers, flight arrays, and cooperative aerial towing or ball juggling (see e.g., [7]–[12]), both relative attitudes and relative positions in a network need to be controlled simultaneously. In this paper, we study coordination problems in 3-D space concerning both relative attitudes and relative positions of a network of agents. The notion *rigid body* is used to express an agent (e.g., spacecraft) in 3-D space with 6 DOFs (see [13]).

At present, there are several typical approaches dealing with rigid-body coordination in 3-D space. One is the decoupled method (see, e.g., [7], [8], [12], and [14]) and its basic idea is to decouple the attitude and position of rigid bodies such that attitude coordination and position coordination can be addressed independently. However, for rigid bodies where the attitude and position are not able to be decoupled due to strong coupling in their dynamics, this approach cannot provide a solution. Another approach is to use homogenous transformation matrices. For example, the approach is adopted in [15] to study attitude synchronization in 3-D space based on passivity theory. Occasional work investigating both attitude and position coordination based on this approach has been reported in recent years except that the homogenous transformation matrix is used to describe the pose of the payload in [11]. Other related techniques addressing both attitude and position in coordination can be found in [16] and [17], which attempt to derive a formal abstraction for a team of robots to control the position, attitude, and shape of the team.

In this paper, we employ unit dual quaternion algebra, which is widely used in the control of manipulators [18], in the synthesis and analysis of coordination strategies for multiple rigid bodies in 3-D space. The objective is to provide a *dual quaternion solution* to the problem of coordinating the attitudes and positions of networked rigid bodies in a *decentralized manner* without causing any singularity by taking advantage of the unit dual quaternion representations. The dual quaternion is a unified mathematical tool to describe the attitude and position of a rigid body simultaneously in 3-D space including three rotational and three translational DOFs. It provides an efficient global representation with concise notions and clear geometric significance in 3-D space without singularity. More comparative studies for different tools to represent the transformation in 3-D space can be found in [19] and [20] and the references therein. In addition, it is expected that the control law for each individual rigid body uses only *local information* from its neighbors. To the best of our knowledge, our work is the first attempt to incorporate unit dual quaternion representations for the study of formation control problems in 3-D space.

To characterize the system behavior of a group of rigid bodies under motion coordination, we introduce a notion called *pairwise asymptotic stability (PAS)*. It means that any two rigid bodies can asymptotically achieve and maintain a desired relative configuration (both attitude and position) although this pair of rigid bodies may not be neighbors and do not interact with each other directly. Although this concept is one just involving a single pair of neighboring agents, it gives rise to stability of the overall system in a straightforward manner. Thus, the basic problem is to find a distributed control strategy together with a certain type of control topology such that a network of rigid bodies holds the property of PAS. It is well known that multiple agents coordination and formation heavily depend on the information architecture assumed for what agents can sense or control (see [6] for an overview). In this paper, we consider a rooted-tree topology, termed *dual quaternion weighted tree*, to describe what each rigid body can sense and control. The dual quaternion weight attributed to an edge specifies the desired relative configuration between the pair of rigid bodies and is the control specification for each rigid body. It will be seen that a fully (complete) connected graph is not necessary and that a rooted tree is the simplest one to ensure PAS. By accessing both relative attitude and relative position information from its neighbor in the rooted tree, each rigid body reacts according to a unit dual quaternion based control law. Thus, the control scheme is scalable and decentralized. We then show that the proposed control strategy together with the rooted-tree topology lead to PAS of rigid bodies in the group. Since a unit dual quaternion provides a global representation for attitude and position transformation simultaneously in 3-D space, our proposed control law and corresponding stability analysis do not have singularity issues. The result is validated by simulations of a seven quad-rotor formation on the Urban Search And Rescue Simulation (USARSim) platform.

While perfect sensing and control are assumed in most existing work, errors are inevitable in practical directed formations. Therefore, we separately investigate an important issue in practical applications—*error*

Manuscript received April 18, 2011; revised August 21, 2011 and December 30, 2011; accepted April 17, 2012. Date of publication June 15, 2012; date of current version September 28, 2012. This paper was recommended for publication by Associate Editor D. Song and Editor G. Oriolo upon evaluation of the reviewers' comments. The work of X. Wang was supported in part by the China Scholarship Council, by the Shandong Key Laboratory of Computer Networks, and by National ICT Australia Ltd. The work of C. Yu was supported by the Australian Research Council through a Queen Elizabeth II Fellowship and DP-110100538 and Overseas Expert Program of Shandong Province. The work of Z. Lin was supported by the National Natural Science Foundation of China under Grant 60875074 and a visitor Grant from DP-0877562. This work was completed during X. Wang's visit to the Australian National University and National ICT Australia Ltd.

X. Wang is with the College of Mechatronics and Automation, National University of Defense Technology, Hunan 410073, China (e-mail: xkwang@nudt.edu.cn).

C. Yu is with the Research School of Engineering, The Australian National University, Canberra, A.C.T. 0200, Australia, and Shandong Computer Science Center, Jinan 250014, China (e-mail: brad.yu@anu.edu.au).

Z. Lin is with the College of Electrical Engineering, Zhejiang University, Hangzhou 310003, China (e-mail: linz@zju.edu.cn).

Color versions of one or more of the figures in this paper are available online at http://ieeexplore.ieee.org.

Digital Object Identifier 10.1109/TRO.2012.2196310

accumulation, i.e., sensing, control, and actuation errors accumulated along a path starting from the lead, if any. To explore the depth conditions on the rooted tree, we re-explain derived formulas in the sense of error accumulation to provide a safety bound on the formation error. The depth conditions can be used to help design a safe topology structure to meet a given error upper-bound specification. Specifically, by considering both angular and distance error thresholds, we obtain an upper bound on the number of rigid bodies allowed to be embodied in each path. This is particularly useful in constructing safe structures for formations with a little prior knowledge. We demonstrate it in detail with a simple example.

II. Mathematical Preliminaries

A *quaternion* is an extension of a complex number to $\mathbb{R}^4$. Formally, a quaternion is defined as $q = [s, \boldsymbol{v}]$, where s is a scalar (called the *scalar part*), and $\boldsymbol{v}$ is a 3-D vector (called the *vector part*). The conjugate of a quaternion q is $q^* = [s, -\boldsymbol{v}]$. For two quaternions $q_1 = [s_1, \boldsymbol{v}_1]$ and $q_2 = [s_2, \boldsymbol{v}_2]$, the *addition* and *multiplication* operations are, respectively, defined as

$$q_1 + q_2 = [s_1 + s_2, \boldsymbol{v}_1 + \boldsymbol{v}_2] \tag{1}$$

$$q_1 \circ q_2 = [s_1 s_2 - \boldsymbol{v}_1^T \boldsymbol{v}_2, s_1 \boldsymbol{v}_2 + s_2 \boldsymbol{v}_1 + \boldsymbol{v}_1 \times \boldsymbol{v}_2]. \tag{2}$$

If $q \circ q^* = Q_I = [1, 0, 0, 0]$, then q is called a *unit quaternion*.

A *dual number* is defined as

$$\hat{a} = a + \epsilon b \text{ with } \epsilon^2 = 0, \text{but } \epsilon \neq 0 \tag{3}$$

where a and b are real numbers, called the *real part* and the *dual part*, respectively, and ϵ is nilpotent such as $\begin{pmatrix} 0 & 1 \\ 0 & 0 \end{pmatrix}$. Given two dual numbers $\hat{v}_1 = v_{r1} + \epsilon v_{d1}$ and $\hat{v}_2 = v_{r2} + \epsilon v_{d2}$, if $v_{r1} - v_{r2} \geq 0$ and $v_{d1} - v_{d2} \geq 0$, then we denote $\hat{v}_1 \geq \hat{v}_2$. The same goes for the definition of operator '$>$'. *Dual vectors* are a generalization of dual numbers whose real and dual parts are both 3-D vectors.

A *dual quaternion* is a quaternion with dual number components, i.e., $\hat{q} = [\hat{s}, \hat{\boldsymbol{v}}]$, where $\hat{s}$ is a dual number and $\hat{\boldsymbol{v}}$ is a dual vector. A 3-D (dual) vector can also be treated equivalently as a (dual) quaternion with vanishing scalar part, called *(dual) vector quaternion*. If not otherwise stated, a (dual) vector is denoted using boldface, and its corresponding (dual) vector quaternion is denoted using normal type, for example, $v = [0, \boldsymbol{v}]$ or $\hat{v} = [0, \hat{\boldsymbol{v}}]$.

A dual quaternion also can be treated as a dual number with quaternion components, i.e., $\hat{q} = q_r + \epsilon q_d$, where q_r and q_d are quaternions. The *conjugate* of a dual quaternion $\hat{q}$ is

$$\hat{q}^* = q_r^* + \epsilon q_d^*. \tag{4}$$

For two dual quaternions $\hat{q}_1$ and $\hat{q}_2$, the *addition* and the *multiplication* operations are defined by

$$\hat{q}_1 + \hat{q}_2 = q_{r1} + q_{r2} + \epsilon(q_{d1} + q_{d2}) \tag{5}$$

$$\hat{q}_1 \circ \hat{q}_2 = q_{r1} \circ q_{r2} + \epsilon(q_{r1} \circ q_{d2} + q_{d1} \circ q_{r2}) \tag{6}$$

respectively. According to (4) and (6), it holds that

$$(\hat{q}_1 \circ \hat{q}_2)^* = \hat{q}_2^* \circ \hat{q}_1^*. \tag{7}$$

If $\hat{q} \circ \hat{q}^* = \hat{Q}_I = [1, 0, 0, 0] + \epsilon[0, 0, 0, 0]$, then the dual quaternion $\hat{q}$ is called a *unit dual quaternion*.

Unit quaternions can be used to describe rotations. For the frame rotation about the unit axis $\boldsymbol{n}$ with an angle $|\theta| < 2\pi$, there is a unit quaternion

$$q = \left[\cos\left(\frac{|\theta|}{2}\right), \sin\left(\frac{|\theta|}{2}\right)\boldsymbol{n}\right] \tag{8}$$

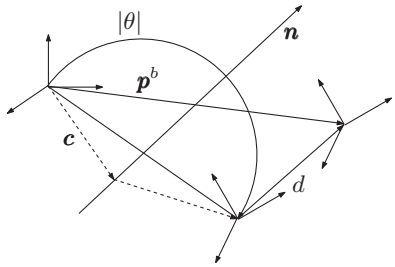

Fig. 1. Geometry of screw motion.

relating a fixed vector expressed in the original frame $\boldsymbol{r}^o$ with the same vector expressed in the new frame $\boldsymbol{r}^n$ by

$$r^n = q^* \circ r^o \circ q. \tag{9}$$

Note that r^o and r^n in (9) are two vector quaternions.

A unit dual quaternion can be used to represent a transformation in 3-D space. Considering a rotation q succeeded by a translation $\boldsymbol{p}^b$, according to the Chasles Theorem ([21], Th. 2.11), this transformation is equivalent to a screw motion, which is a rotation about an axis $\boldsymbol{n}$ with angle $|\theta|$ combined with a translation d parallel to $\boldsymbol{n}$ illustrated in Fig. 1. The transformation can be represented using a unit dual quaternion[1]

$$\hat{q} = \left[\cos\frac{\hat{\theta}}{2}, \sin\frac{\hat{\theta}}{2}\hat{\boldsymbol{n}}\right] = q + \frac{\epsilon}{2} q \circ p^b \tag{10}$$

where $\hat{\boldsymbol{n}} = \boldsymbol{n} + \epsilon(\boldsymbol{c} \times \boldsymbol{n})$ is the screw axis, in which $\boldsymbol{c}$ is the vector from the original position to the rotational center (see Fig. 1), and $\hat{\theta} = |\theta| + \epsilon d$ is the dual angle of the screw [22].

The logarithm of a unit quaternion given in (8) is defined as [23]

$$\ln q = \frac{|\theta|}{2}\boldsymbol{n}. \tag{11}$$

Similarly, the logarithmic mapping of a unit dual quaternion given by (10) is defined as [24]

$$\ln \hat{q} = \frac{1}{2}(\theta + \epsilon p^b) \tag{12}$$

where $\theta = [0, \boldsymbol{\theta}]$ with $\boldsymbol{\theta} = |\theta|\boldsymbol{n}$, and $p^b = [0, \boldsymbol{p}^b]$.

Given a (dual) vector quaternion v ($\hat{v}$) and a unit (dual) quaternion q ($\hat{q}$), the *adjoint transformation* is defined as

$$Ad_q v = q \circ v \circ q^* \quad \text{or} \quad Ad_{\hat{q}} \hat{v} = \hat{q} \circ \hat{v} \circ \hat{q}^*. \tag{13}$$

As noted earlier, a unit quaternion q defines a rotation, taking coordinates of a point from one frame to another. Conversely, every attitude of a rigid body that is free to rotate relative to a fixed frame can be identified with a unique unit quaternion q. Analogously to the rotational case, a unit dual quaternion $\hat{q}$ serves as both a specification of the configuration of a rigid body and a transformation taking the coordinates of a point from one frame to another via rotation and translation. These ideals come together nicely in the following property.

Property 1: If the configurations of rigid bodies i and j are $\hat{q}_i$ and $\hat{q}_j$, and the transformation (relative configuration) from rigid body i to j is $\hat{q}_{ij}$, then $\hat{q}_j = \hat{q}_i \circ \hat{q}_{ij}$.

[1]Superscripts b and s relate to the body frame (which is attached to the rigid body) and the spatial frame (which is relative to a fixed (inertial) coordinate frame), respectively, throughout this paper. The concepts of body frame and spatial frame come from [21].

Consider two unit dual quaternions $\hat{q}$ and $\hat{q}_d$ defined as in (10). The *left-invariant error* from $\hat{q}$ to $\hat{q}_d$ is

$$\hat{q}_e = \hat{q}_d^* \circ \hat{q} = q_e + \frac{\epsilon}{2} q_e \circ p_e^b \tag{14}$$

where $q_e = q_d^* \circ q$, and $p_e^b = p^b - Ad_{q_e^*} p_d^b$. The left-invariant error describes the relative configuration or the mismatch between two configurations in terms of unit dual quaternions. It should be noted that if $\hat{q}_e = \pm \hat{Q}_I$, then $\hat{q} = \hat{q}_d$.

III. Problem Formulation

Consider the motion of a group of $n+1$ rigid bodies in 3-D space with the kinematics expressed by unit dual quaternions, i.e.,

$$\dot{\hat{q}}_i = \frac{1}{2} \hat{q}_i \circ \xi_i^b, i = 0, \ldots, n \tag{15}$$

where the unit dual quaternion

$$\hat{q}_i = q_i + \frac{\epsilon}{2} q_i \circ p_i^b \tag{16}$$

represents the configuration of rigid body i (including attitude q_i and position $\boldsymbol{p}_i^b$), and the dual vector quaternion

$$\xi_i^b = \omega_i^b + \epsilon(\dot{p}_i^b + \omega_i^b \times p_i^b) \tag{17}$$

is the *twist* of rigid body i (including the angular velocity $\boldsymbol{\omega}_i^b$ and the linear velocity $\dot{\boldsymbol{p}}_i^b$) [22]. A quite different approach to capture the kinematics relevant to attitude synchronization in 3-D space is provided in [15], in which the kinematics are represented by the homogeneous transformation matrices.

Remark 1: Conventionally, for a typical flying robot, quad-rotor, its dynamics with four inputs is differentially flat, and its corresponding control space has one rotational DOF and three translational DOFs, which is isomorphic to $SO(2) \otimes \mathbb{R}^3$ (for details refer to [25], [26]). Correspondingly, taking the z-axis as the rotational axis, the configuration and the twist given in (16) and (17) can be specified in this control space by

$$\begin{aligned} \hat{q}_i =& [\cos\frac{\theta_{zi}}{2}, 0, 0, \sin\frac{\theta_{zi}}{2}] \\ &+ \frac{\epsilon}{2}[\cos\frac{\theta_{zi}}{2}, 0, 0, \sin\frac{\theta_{zi}}{2}] \circ [0, x_i^b, y_i^b, z_i^b] \end{aligned} \tag{18}$$

and

$$\begin{aligned} \boldsymbol{\xi}_i^b =& (0, 0, \omega_{zi}^b) \\ &+ \epsilon\big((\dot{x}_i^b, \dot{y}_i^b, \dot{z}_i^b) + (0, 0, \omega_{zi}^b) \times (\dot{x}_i^b, \dot{y}_i^b, \dot{z}_i^b)\big) \end{aligned} \tag{19}$$

respectively, where the angle θ_{zi} and angular velocity ω_{zi}^b relate to $SO(2)$, and the position (x_i^b, y_i^b, z_i^b) and linear velocity $(\dot{x}_i^b, \dot{y}_i^b, \dot{z}_i^b)$ relate to $\mathbb{R}^3$.

Throughout the paper, we call a group of rigid bodies with the kinematics expressed by (15)–(17) the *overall system*. In many applications, such as space-based interferometers, and multiple spacecraft formation flying, all the relative configurations between any two rigid bodies are required to be maintained. To illustrate this property of the overall system, we need to define one new stability notion regarding any pair of rigid bodies in the group, termed *PAS*. Denote the desired and actual relative configurations from rigid body i to rigid body j by $\hat{q}_{d_{ij}}$ and $\hat{q}_{ij} = \hat{q}_i^* \circ \hat{q}_j$ ($i, j \in \{0, \ldots, n\}$ and $i \neq j$), respectively.

Definition 1 (PAS): For **any pair** of rigid bodies i and j in the overall system, if the actual relative configuration $\hat{q}_{ij}$ converges to the desired relative configuration $\hat{q}_{d_{ij}}$ asymptotically, viz., when $t \to \infty$, $\hat{q}_{ij}(t) \to \hat{q}_{d_{ij}}$, then we say that the overall system is pairwise asymptotically stable.

Remark 2: The leader-to-formation stability (LFS) concept defined in [27] builds on the notion of input-to-state stability and includes both transient and steady-state errors, while the PAS only reflects the asymptotic stability of steady-state errors. If any pair of rigid bodies can maintain their relative configuration asymptotically, i.e., the overall system is PAS, then it is obvious that the overall system is LFS with zero inputs.

PAS means that the desired relative configuration between any pair of rigid bodies can be achieved. Given any arbitrary desired formation defined by the desired relative configurations between rigid bodies, a group of rigid bodies can achieve the desired formation by using the concept of PAS. Therefore, although this concept is one just involving a single pair of neighboring agents, it gives rise to stability of the overall system as a straightforward consequence. Note that the definition makes no mention of designated control links in the overall system, and the group of rigid bodies can achieve a unique desired formation by using the concept of PAS together with certain topology. Consequently, to make the overall system achieve PAS, there is no implication that one must design a control law between every pair of rigid bodies. What we do need is to design a control interconnection structure defined by neighbor relationships and the distributed control law based on this structure, such that all the desired relative configurations for any two rigid bodies in the overall system are satisfied. In the sequel, the goals of this paper can be formulated into two problems.

Problem 1: To design a distributed control strategy together with a control interconnection graph (of certain topology) so that the overall system achieves PAS.

Problem 2: To find the depth conditions on the control interconnection graphs, such that a given safety bound on the formation error can be satisfied in the presence of error accumulation along every path.

IV. Control Strategy and Stability Analysis

We first solve Problem 1.

A. Control Interconnection Graph and Control Strategy

In [5], it is proven that formation stabilization is feasible if and only if the sensor graph has a globally reachable node. The rooted tree is the most fundamental and simplest digraph, including a globally reachable node. In addition, in our setup, we note that the rooted tree is the simplest digraph to solve Problem 1 and requires the least cost in communication/sensing.

On the rooted tree, we attribute to each arc the desired relative configuration between two neighboring rigid bodies represented by a unit dual quaternion. Such a rooted tree is called a *dual quaternion weighted tree* and is denoted by $G = (V, E, Q)$, where $V := \{0, 1, \ldots, n\}$ is the set of nodes representing rigid bodies, $E := \{e_{ij}\}$ is the set of arcs describing the control interconnections, and $Q := \{\hat{q}_{d_{ij}}\}$ is the set of dual quaternion weights with each associated with an arc specifying the desired relative configuration. For an arc e_{ij}, node i is its tail and node j is its head, meaning that rigid body j is expected to maintain the desired relative configuration $\hat{q}_{d_{ij}}$ with respect to rigid body i. In the rooted tree, there is only one *lead*—the one without neighbors, and except for the lead, each rigid body has only one *neighbor*. The nodes which are not neighbors of any other nodes are called *leaf nodes*. An illustrative example, a dual quaternion weighted tree for a group of seven rigid bodies, is shown in Fig. 2. In this example, rigid body 0 is the lead, and 1, 3, 4, and 6 are the leaf nodes.

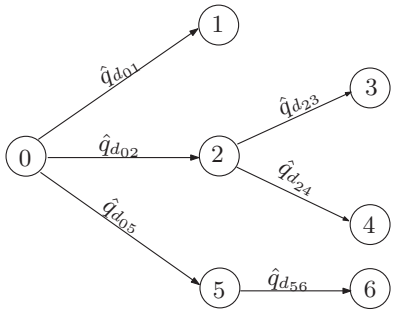

Fig. 2. Dual quaternion weighted tree.

The control strategy is then set up based on the dual quaternion weighted tree. Consider a pair of neighbors i and j in the rooted tree with the desired specification $\hat{q}_{d_{ij}}$ in the overall system. According to the widely used virtual structure method, the control law design can be composed of two steps: 1) formulating the trace of a virtual rigid body j', which can maintain the desired relative configuration and has the same twist of rigid body i all the time; and 2) designing a local control law to track the trace of virtual rigid body j'.

For the first step, it follows from Property 1 that if the trace and the twist of rigid body i are $\hat{q}_i$ and ξ_i^b, respectively, then the trace and the twist of the virtual rigid body j' should be

$$\hat{q}_{j'} = \hat{q}_i \circ \hat{q}_{d_{ij}} \tag{20}$$

and

$$\xi_{j'}^b = \xi_i^b. \tag{21}$$

For the second step, we first denote

$$\hat{q}_{e_{j'j}} = \hat{q}_{j'}^* \circ \hat{q}_j \tag{22}$$

as the left-invariant error from rigid body j to the virtual rigid body j'. A generalized proportional control law with the logarithm feedback of unit dual quaternion is then available from [28] for tracking, i.e.,

$$\xi_j^b = Ad_{\hat{q}_{e_{j'j}}}(\xi_{j'}^b + 2\hat{k}_j \cdot \ln \hat{q}_{e_{j'j}}) \tag{23}$$

where $\hat{\boldsymbol{k}}_j = \boldsymbol{k}_{rj} + \epsilon \boldsymbol{k}_{dj}$ is a dual vector with each component greater than 0, and the symbol '$\cdot$' is the *dot-product* between two dual vector quaternions, which is defined as follows:

Definition 2 (Dot-product): Let $\hat{v} = [0, \boldsymbol{v}_r] + \epsilon[0, \boldsymbol{v}_d]$ and $\hat{k} = [\hat{0}, \hat{\boldsymbol{k}}]$ with $\hat{\boldsymbol{k}} = (k_{r1}, k_{r2}, k_{r3})^T + \epsilon(k_{d1}, k_{d2}, k_{d3})^T$ be dual vector quaternions, and denote $K_r = \text{diag}(k_{r1}, k_{r2}, k_{r3})$ and $K_d = \text{diag}(k_{d1}, k_{d2}, k_{d3})$. Then, $\hat{k} \cdot \hat{v} = [0, K_r \boldsymbol{v}_r] + \epsilon[0, K_d \boldsymbol{v}_d]$.

Substituting (20) into (22), and noting that $\hat{q}_i^* \circ \hat{q}_j = \hat{q}_{ij}$, we obtain

$$\hat{q}_{e_{j'j}} = \hat{q}_{d_{ij}}^* \circ \hat{q}_i^* \circ \hat{q}_j = \hat{q}_{d_{ij}}^* \circ \hat{q}_{ij}. \tag{24}$$

Substituting (21) and (24) into (23), a general formation control law for each rigid body j in the rooted tree except the lead is obtained:

$$\xi_j^b = Ad_{(\hat{q}_{d_{ij}}^* \circ \hat{q}_{ij})}(\xi_i^b + 2\hat{k}_j \cdot \ln(\hat{q}_{d_{ij}}^* \circ \hat{q}_{ij})) \tag{25}$$

where rigid body i is the neighbor of rigid body j.

Control law (25) provides a dual quaternion solution for the attitude and position control of a group of rigid bodies in 3-D space with notional conciseness and no singularity. Moreover, ξ_i^b is the neighbor's twist, and $\hat{q}_{ij}$ and $\hat{q}_{d_{ij}}$ are, respectively, the actual and desired relative configurations along a path of the dual quaternion weighted tree as rigid body i is the neighbor of j. Specially, configurations $\hat{q}_{ij}$ and $\hat{q}_{d_{ij}}$ can be obtained directly from q_{ij} and $\boldsymbol{p}_{ij}^b$, as well as $q_{d_{ij}}$ and $\boldsymbol{p}_{d_{ij}}^b$ by

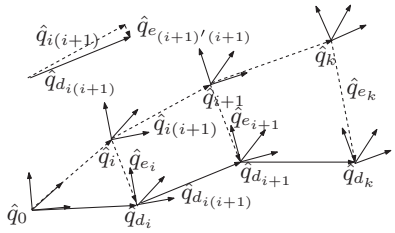

Fig. 3. Illustration of rigid bodies in on path.

using (10), respectively; q_{ij} and $q_{d_{ij}}$ are the actual and desired relative attitudes respectively, and $\boldsymbol{p}_{ij}^b$ and $\boldsymbol{p}_{d_{ij}}^b$ are the actual and desired relative positions, respectively. It should be noted that for rigid body i, the required q_{ij} and $\boldsymbol{p}_{ij}^b$ are only local information from its neighbor. Therefore, control law (25) is distributed, i.e., only requires the rigid body's own information and that of its neighbor, and scalable without increasing the complexity of measurements or communications.

Remark 3: The control law used is a generalized proportional control scheme based on the logarithmic mapping. Similar logarithmic mapping based control law in SE(3) for a single rigid body transformation control can be found in [29]; with homogenous representations, the proportional control is also used in [15] to cause the attitudes of multiple rigid bodies to synchronize. Some other types of control laws based on the unit dual quaternion, such as generalized proportional–integral–derivative control [30] and feedback linearization control [31], could be applied to solve the problem too.

B. Stability Analysis

In the sequel, we will analyze the stability property of the overall system under control law (25) with a dual quaternion weighted tree.

We first construct a path in the dual quaternion weighted tree. Denote the rigid bodies in the path by rigid body $0, \ldots, i, i+1, \ldots, k (0 \leq i < k)$, where rigid body 0 is the lead, rigid body k is the leaf node, and rigid body i is the neighbor of rigid body $i+1$. For $i = 0, \ldots, k-1$, denote the desired and actual relative configurations from rigid body $i+1$ to rigid body i (shown in Fig. 3), respectively, by $\hat{q}_{d_{i(i+1)}} = q_{d_{i(i+1)}} + \frac{\epsilon}{2} q_{d_{i(i+1)}} \circ p_{d_{i(i+1)}}^b$ and $\hat{q}_{i(i+1)} = q_{i(i+1)} + \frac{\epsilon}{2} q_{i(i+1)} \circ p_{i(i+1)}^b$. Because of errors, the actual relative configuration cannot coincide with the desired relative configuration. Correspondingly, from (14), the mismatch (left-invariant error) at rigid body $i+1$, which is denoted by $\hat{q}_{e_{(i+1)'(i+1)}}$, is

$$\begin{aligned} \hat{q}_{e_{(i+1)'(i+1)}} &= \hat{q}_{d_{i(i+1)}}^* \circ \hat{q}_{i(i+1)} \\ &= q_{e_{(i+1)'(i+1)}} + \frac{\epsilon}{2} q_{e_{(i+1)'(i+1)}} \circ p_{e_{(i+1)'(i+1)}}^b \end{aligned} \tag{26}$$

where $q_{e_{(i+1)'(i+1)}} = q_{d_{i(i+1)}}^* \circ q_{i(i+1)}$, and $p_{e_{(i+1)'(i+1)}}^b = p_{i(i+1)}^b - Ad_{q_{e_{(i+1)'(i+1)}}^*} p_{d_{i(i+1)}}^b$.

For $i = 0, \ldots, k-1$, from Property 1, the actual and the desired configurations of rigid body i are

$$\hat{q}_{i+1} = \hat{q}_0 \circ \hat{q}_{01} \circ \ldots \circ \hat{q}_{(i-1)i} \circ \hat{q}_{i(i+1)} \tag{27}$$

$$\hat{q}_{d_{i+1}} = \hat{q}_0 \circ \hat{q}_{d_{01}} \circ \ldots \circ \hat{q}_{d_{(i-1)i}} \circ \hat{q}_{d_{i(i+1)}}. \tag{28}$$

Immediately the left-invariant error form rigid body 0 to k, which is denoted by $\hat{q}_{e_k} = \hat{q}_{d_k}^* \circ \hat{q}_k$, can be represented in an iterative form as follows:

$$\hat{q}_{e_1} = \hat{q}_{e_1'1} \tag{29}$$

$$\hat{q}_{e_{i+1}} = Ad_{\hat{q}_{d_{i(i+1)}}^*} \hat{q}_{e_i} \circ \hat{q}_{e_{(i+1)'(i+1)}}, i = 1, \ldots, k-1. \tag{30}$$

Obviously, to prove the overall system is PAS, it is necessary to show that $\hat{q}_{e_{i+1}} \to \pm\hat{Q}_I$. To measure the errors in (29)–(30), we introduce a *Logarithmic Norm* of a unit dual quaternion, which ensures that when $|\ln \hat{q}_{e_{i+1}}| = 0 + \epsilon 0$, $\hat{q}_{e_{i+1}} = \pm\hat{Q}_I$.

Definition 3 (Logarithmic Norm): The logarithmic norm of $\hat{q}$ represented in (10) is defined by $|\ln \hat{q}| = |\boldsymbol{\theta}| + \epsilon|\boldsymbol{p}^b|$.

For $i = 0, \ldots, k-1$, let $\Theta_i = \sum_{j=1}^{i} |\boldsymbol{\theta}_{e_{j'j}}|$, where $\theta_{j'j}$ is from the real part of $\ln \hat{q}_{e_{j'j}}$ defined in (12). We are usually interested in the case that the Θ_i are all less than π since otherwise, the accumulation of errors is quite big, distorting the desired formation severely. In this case, an upper bound on $|\ln \hat{q}_{e_k}|$ in (29)–(30) can be obtained, as stated in Lemma 1.

Lemma 1: If $\Theta_j \leq \pi, \forall j = 1, \ldots, k$, from (29)–(30), the following upper bound for $|\ln \hat{q}_{e_k}|$ holds.

$$|\ln \hat{q}_{e_k}| \leq \Theta_k + \epsilon \left(\sum_{i=1}^{k} |\boldsymbol{p}^b_{e_{i'i}}| + 2 \sum_{j=1}^{k-1} |\boldsymbol{p}^b_{d_{j(j+1)}}| \sin \frac{\Theta_j}{2} \right). \quad (31)$$

The proof is in Appendix A.

With the above lemma, the asymptotic behavior from any rigid body k to the lead is then provided in Theorem 1 with proof in Appendix B.

Theorem 1: For any path $(0, \ldots, k)$ in the dual quaternion weighted tree under the control law (25), we obtain $\hat{q}_k(t) \to \hat{q}_{d_k}$ when $t \to \infty$.

Finally, let us consider two arbitrary rigid bodies i and j in the overall system. Clearly, in the rooted tree, rigid body 0 is followed both by rigid bodies i and j, hence two paths $(0, \ldots, i)$ and $(0, \ldots, j)$ can be constructed in the dual quaternion weighted tree correspondingly. According to Property 1, we obtain

$$\hat{q}_{ij} = \hat{q}_i^* \circ \hat{q}_j \text{ and } \hat{q}_{d_{ij}} = \hat{q}_{d_i}^* \circ \hat{q}_{d_j}. \quad (32)$$

Now we can present our main result.

Theorem 2: The overall system under control law (25) with a dual quaternion weighted tree is PAS.

The proof of Theorem 2 is in Appendix C.

Theorem 2 indicates that any pair of rigid bodies in the group can track its desired relative configuration asymptotically, and the global asymptotic stability of the overall system is achieved. Note that what we do to guarantee the overall system achieving PAS is to design a distributed control strategy [control law (25)] with a specified control interconnection graph (rooted tree), and any two rigid bodies can asymptotically achieve and maintain the desired relative configuration no matter they are neighbors or interact directly. Further, this stability holds no matter whether the lead is stationary or moving. If the lead is at rest, then control law (25) causes the overall system to form the desired static formation, whereas if the lead is moving, then the achieved formation moves as a cohesive whole.

C. Case Study

For visualization, we verify the proposed control strategy on the USARSim platform with seven quad-rotor models (refer to http://usarsim.sourceforge.net for details of USARSim and the quad-rotor model). It should be noted that although the control space of quad-rotor is isomorphic to $SO(2) \otimes \mathbb{R}^3$, the couplings between attitude and position still hold. The dual quaternion weighted tree is shown in Fig. 2 and the control law is (25) for each rigid body $j \in \{1, \ldots, 6\}$.

For convenience and clarity, we employ $(\theta^s_{zi}, x^s_i, y^s_i, z^s_i)$ and $(\omega^s_{zi}, \dot{x}^s_i, \dot{y}^s_i, \dot{z}^s_i)$ to denote the quad-rotor i's $(i = 0, \ldots, 6)$ configuration and twist in spatial frame, respectively. The corresponding representations $(\theta^b_{zi}, x^b_i, y^b_i, z^b_i)$ and $(\omega^b_{zi}, \dot{x}^b_i, \dot{y}^b_i, \dot{z}^b_i)$ in body frame can be obtained by using (9) from $(\theta^s_{zi}, x^s_i, y^s_i, z^s_i)$ and $(\omega^s_{zi}, \dot{x}^s_i, \dot{y}^s_i, \dot{z}^s_i)$, respectively. In the simulation setup, each quad-rotor is with flight stabilization control and can be controlled directly by $(\omega^b_{zj}, \dot{x}^b_j, \dot{y}^b_j, \dot{z}^b_j)$ for $j \in \{1, \ldots, 6\}$; further, the attitude, position, linear velocity, and angular velocity information of each quad-rotor in body frame can be obtained real time, which implies $\hat{q}_{ij}$ and $\boldsymbol{\xi}^b_i$ is available. By using control law (25) with the specified $\hat{q}_{d_{ij}}$ and $\hat{\boldsymbol{k}}_j$, the control input $\boldsymbol{\xi}^b_j$ is obtained for each quad-rotor j. It should be noted that when applying dual quaternion descriptors (18) and (19) in the control law (25), the first and second elements of $\boldsymbol{\xi}^b_j$ are both zero; thus, $(\omega^b_{zj}, \dot{x}^b_j, \dot{y}^b_j, \dot{z}^b_j)$ is obtained naturally from $\boldsymbol{\xi}^b_j$ and can be provided to the quad-rotor model to control the behaviors of quad-rotor j.

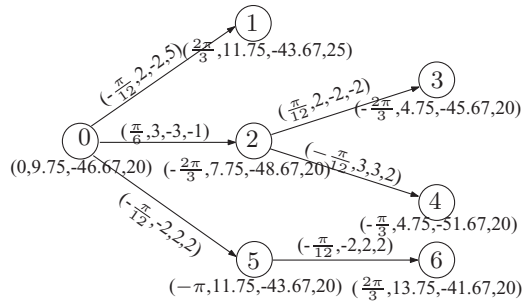

Fig. 4. Rooted tree with the initial configurations (below the nodes) and the desired relative configurations (on the links between nodes) between quad-rotors.

The lead (quad-rotor 0) tracks a reference trajectory, denoted by $(\theta^s_{d_{z0}}, x^s_{d_0}, y^s_{d_0}, z^s_{d_0})$, as follows:

$$\begin{cases} \theta^s_{d_{z0}}(t) = a_1 t + \alpha \\ x^s_{d_0}(t) = r\cos\theta^s_{d_{z0}}(t) + b_1 \\ y^s_{d_0}(t) = r\sin\theta^s_{d_{z0}}(t) + b_2 \\ z^s_{d_0}(t) = c\sin(a_2 t) + b_3 \end{cases} \quad (33)$$

with $a_1 = 0.1$ /s, $a_2 = 0.1$ /s, $r = 10$ m, $c = 5$ m, $\alpha = \pi/3$, $b_1 = 8$ m, $b_2 = -46.67$ m, and $b_3 = 25$ m.

In the simulation, the used desired relative configurations between quad-rotors and the initial configurations are shown in Fig. 4. At the beginning of the simulation, all quad-rotors are at rest. The parameters in (25) are all the same, viz., $\hat{\boldsymbol{k}}_j = (0, 0, 0.2)^T + \epsilon(1.0, 1.0, 1.0)^T, (j = 1, \ldots, 6)$. A video of the simulation is available on http://users.cecs.anu.edu.au/~bradyu/TRO.html, and some results are presented in Figs. 5–7.

Fig. 5 shows the trajectories of quad-rotors (for clear illustration, a video animation of Fig. 5 is available on http://users.cecs.anu.edu.au/~bradyu/TRO.html). To illustrate the fine structure clearly, the actual trajectory and the desired trajectory of each quad-rotor in $(\theta^s, x^s, y^s, z^s)$ are further shown in Fig. 6. In simulation, the desired formation is achieved; and in the end, the formation moves as a cohesive whole. All quad-rotors track their neighbor in the rooted tree in Fig. 2 asymptotically under the control law (25), and all errors between any two quad-rotors also converge to 0 asymptotically (PAS). Some typical relative errors in attitude and position are shown in Fig. 7.

V. Error Accumulation and Formation Design

We can construct different rooted trees for the control interconnection of the overall system; Theorem 2 shows that all the rooted trees ensure the overall system is PAS under control law (25). However, errors are inevitable in practical applications, and can be accumulated along the paths in the rooted trees. Thus, considering a safety bound on

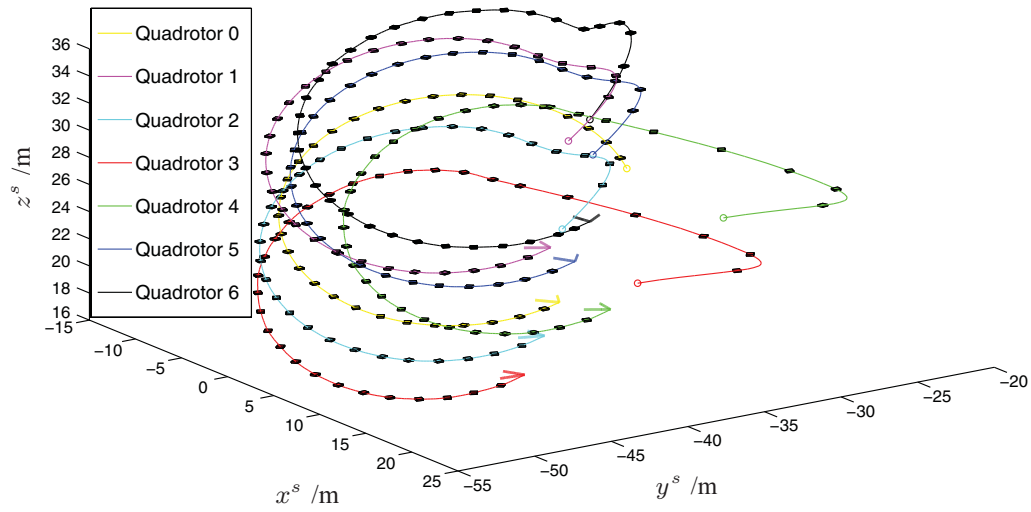

Fig. 5. Trajectories of seven quad-rotors in 3-D space in which circles denote the initial positions, and arrows indicate the final positions and attitudes.

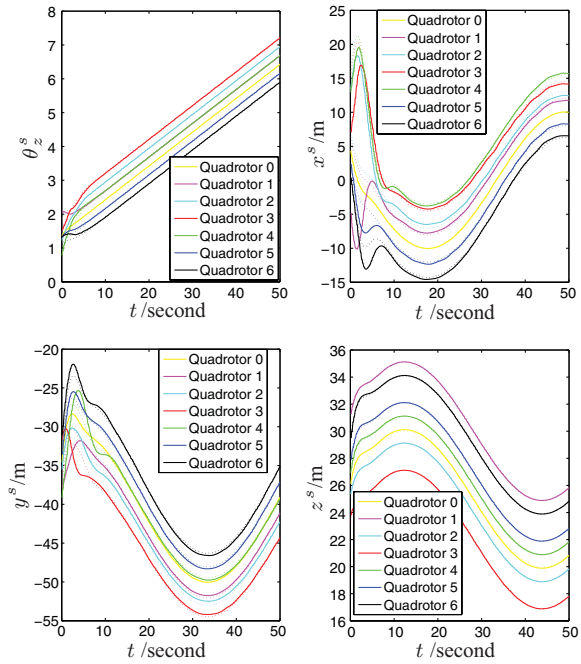

Fig. 6. Trajectories of seven quad-rotors in $(\theta_z^s, x^s, y^s, z^s)$.

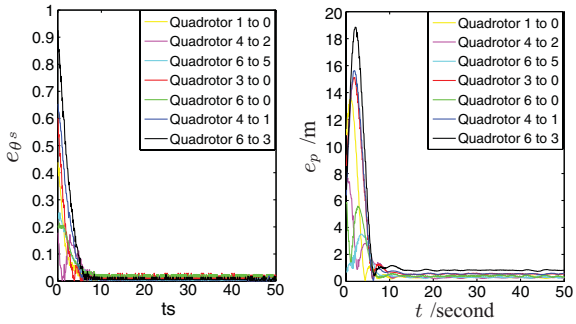

Fig. 7. Some typical errors in attitude and position.

the formation error, another separate but important issue (*Problem 2*) is to find some conditions to guide the structure design for the rooted trees such that the given bound can be satisfied.

Let us reinvestigate some formulas, especially, Lemma 1, in Section IV-B in the sense of error accumulation. In (30), the terms $Ad_{\hat{q}^*_{d_{i(i+1)}}}\hat{q}_{e_i}$ and $\hat{q}_{e_{(i+1)'(i+1)}}$ can be understood as the accumulation of errors from rigid body i to $i+1$ and the errors accruing in rigid body $i+1$, respectively. Thus, $\hat{q}_{e_{i+1}}$ represents error accumulation from rigid body 0 to $i+1$ along the path $(0,\ldots,i+1)$. Consequently, the quantity $|\ln \hat{q}_{e_i}| = |\boldsymbol{\theta}_{e_i}| + \epsilon|\boldsymbol{p}^b_{e_i}|$ describes the amplitude of the error in rotation and translation, where $|\boldsymbol{\theta}_{e_i}|$ is the angular error and $|\boldsymbol{p}^b_{e_i}|$ is the distance error. Thus, the real part and dual part in the right-hand side of (31) provide the upper bounds on distance error and angular error, respectively.

In the sense of error accumulation, Lemma 1 provides a safety bound on the formation error. Given a set of initial conditions and the local errors on each rigid body, one can estimate an upper bound on the errors' accumulation that can keep the system safe. Conversely, given a safety specification, i.e., an angular error threshold T_a and a distance error threshold T_d, we are able to estimate the maximal number of rigid bodies allowed to be embodied in one path for the formation, denoted by $N_{\max}$, such that the overall system's trajectories remain safe at all times. To obtain $N_{\max}$, we first find two maximal integers, which are denoted by N_a and N_d, satisfying the angular and distance error thresholds, respectively. That is, N_a and N_d should satisfy the following inequalities:

$$\begin{cases} \Theta_{N_a} \leq T_a < \Theta_{N_a+1} \\ \sum_{i=1}^{N_d} |\boldsymbol{p}^b_{e_{i'i}}| + 2\sum_{j=1}^{N_d-1} |\boldsymbol{p}^b_{d_{j(j+1)}}| \sin\frac{\Theta_j}{2} \leq T_d \\ \sum_{i=1}^{N_d+1} |\boldsymbol{p}^b_{e_{i'i}}| + 2\sum_{j=1}^{N_d} |\boldsymbol{p}^b_{d_{j(j+1)}}| \sin\frac{\Theta_j}{2} > T_d \end{cases} \tag{34}$$

where $\Theta_j = \sum_{i=1}^{j} |\boldsymbol{\theta}_{e_{i'i}}|$. Then, considering the lead, we obtain

$$N_{\max} = \min(N_a, N_d) + 1. \tag{35}$$

Note that $N_{\max}$ obtained from (34) and (35) also can be treated as the maximum depth of the rooted trees. Although the value $N_{\max}$ may be quite conservative, essentially due to its reflecting the nonstrict inequality of Lemma A.1, it provides a rough estimate for the maximum number of rigid bodies allowed to be embodied in each path, or the maximum depth of the rooted tree, with a prior knowledge of errors $|\boldsymbol{\theta}_{e_{i'i}}|$, $|\boldsymbol{p}^b_{e_{i'i}}|$ and $|\boldsymbol{p}^b_{d_{j(j+1)}}|$. Therefore, it is useful in formation design to construct the appropriate rooted tree satisfying the given safety bound.

In the following, we give a simple example. We assume that all $\hat{q}_{d_{i(i+1)}}$ s in (30) have the same logarithmic norm, that is, $|\ln \hat{q}_{d_{i(i+1)}}| = \alpha + \epsilon d$ with $\alpha, d \geq 0$, and we assume that the angular error and the distance error acting on each rigid body i are no more than $10\%\alpha$ and $10\%d$, respectively, i.e., $|\boldsymbol{\theta}_{e_{i'i}}| \leq 10\%\alpha$ and $|\boldsymbol{p}^b_{e_{i'i}}| \leq 10\%d$. Then, given the safety specifications $T_a = \alpha/2$ and $T_d = d/2$, respectively,[2] when $\alpha = 15\pi/180$, according to (34) and (35), it is easy to obtain $N_{\max} = 4$. Obviously, $N_{\max}$ is nondecreasing with respect to α, and therefore, when $\alpha < 15\pi/180$, we have $N_{\max} \geq 4$. Thus, when $\alpha \leq 15\pi/180$, if the depth of the rooted tree is no more than 4, then the given safety specifications T_a and T_d can be satisfied. Therefore, the dual quaternion weighted tree in Fig. 2 is an appropriate control interconnection graph (with the depth is 3) for an overall system with aforementioned assumptions.

VI. Conclusion and Future Work

In this paper, we have investigated the multiple rigid body coordination in 3-D space based on the unit dual quaternion algebra. We develop a unit dual quaternion based distributed control strategy together with a rooted tree control interconnection and analyze the stability of the overall system with a newly defined notion PAS. We have also explored how to find a maximum depth for the rooted tree such that a given safety bound on the formation error is satisfied by utilizing unit dual quaternion algebra to represent the error accumulation along a path from the lead to the leaf nodes.

Some future work can be envisaged along the direction of this study. The control law design and the related stability analysis from a connected but nontree topology, switching topology, and noise measurements to more challenging issues, such as time delay and having lesser available information (such as only relative distances and angles), will be further explored. In addition, it is desirable to study the self-tuning problem for the proposed control strategy. Finally, the upper bound on the number of rigid bodies allowed to be embodied in each path obtained in this paper is quite conservative. Improving the upper bound estimation is another desirable future task.

Appendix A
Proof of Lemma 1

To prove Lemma 1, let us first note some properties of the logarithmic norm of the unit (dual) quaternion, which can be verified by direct computations, and provide a lemma that will be used in the proof.

Property A.1: Let q_1 and q_2 be two unit quaternions. Then

$$|\ln q_2| = |\ln(Ad_{q_1} q_2)| = |\ln(Ad_{q_1^*} q_2)|.$$

Property A.2: Let q be a unit quaternion, $\theta = 2\ln q$, and $\boldsymbol{p}$ be a 3-D vector. Then, $|\boldsymbol{p} - Ad_q p| \leq 2|\boldsymbol{p}| \sin \frac{|\boldsymbol{\theta}|}{2}$.

Property A.3: Given two unit dual quaternions $\hat{q}_1$ and $\hat{q}_2$, the following inequality holds: $|\ln(\hat{q}_1 \circ \hat{q}_2)| \leq |\ln \hat{q}_1| + |\ln \hat{q}_2|$.

[2] $10\%\alpha$,$10\%d$, $\alpha/2$, and $d/2$ are our preassumptions, which certainly can be varied in practice.

Lemma A.1: Let $\hat{q}_1$, $\hat{q}_2$, and $\hat{q}_3$ are all unit dual quaternions defined in (16), and $\ln \hat{q}_i = \frac{1}{2}(\theta_i + \epsilon p_i^b), i = 1, 2, 3$. Then

$$|\ln(Ad_{\hat{q}_1^*} \hat{q}_2 \circ \hat{q}_3)| \leq |\ln \hat{q}_2| + |\ln \hat{q}_3| + 2\epsilon|\boldsymbol{p}_1^b| \sin \frac{|\boldsymbol{\theta}_2|}{2}.$$

Proof: By direct computations, we obtain

$$\begin{aligned} Ad_{\hat{q}_1^*} \hat{q}_2 =& Ad_{q_1^*} q_2 \\ &+ \frac{\epsilon}{2} Ad_{q_1^*} q_2 \circ (Ad_{q_1^*} p_2^b - Ad_{(Ad_{q_1^*} q_2)^*} p_1^b + p_1^b). \end{aligned} \tag{36}$$

According to Property A.3, we obtain

$$|\ln(Ad_{\hat{q}_1^*} \hat{q}_2 \circ \hat{q}_3)| \leq |\ln(Ad_{\hat{q}_1^*} \hat{q}_2)| + |\ln \hat{q}_3|. \tag{37}$$

Substituting (36) into (37), and then using Property A.1 and A.2, we obtain

$$\begin{aligned} |\ln(Ad_{\hat{q}_1^*} \hat{q}_2 \circ \hat{q}_3)| &\leq |\ln \hat{q}_2| + |\ln \hat{q}_3| + \epsilon(|\boldsymbol{p}_1^b - Ad_{(Ad_{q_1^*} q_2)^*} p_1^b|) \\ &\leq |\ln \hat{q}_2| + |\ln \hat{q}_3| + 2\epsilon|\boldsymbol{p}_1^b| \sin \frac{|\boldsymbol{\theta}_2|}{2}. \end{aligned}$$

■

Now, by an iterative usage of Lemma A.1, we can prove the result of Lemma 1.

Proof of Lemma 1: We use induction to prove the lemma.

1) When $k = 1$, we have $\hat{q}_{e_1} = \hat{q}_{e_{1'1}}$, and therefore
$$|\ln \hat{q}_{e_1}| = |\ln \hat{q}_{e_{1'1}}| = |\theta_{e_{1'1}}| + |p_{e_{1'1}}|.$$
Thus, Lemma 1 is correct when $k = 1$.
2) Assume that Lemma 1 holds for $k = N$. Then, we have
$$|\ln \hat{q}_{e_N}| \leq \Theta_N + \epsilon\Big(\sum_{i=1}^{N} |\boldsymbol{p}^b_{e_{i'i}}| + 2\sum_{j=1}^{N-1} |\boldsymbol{p}^b_{d_{j(j+1)}}| \sin \frac{\Theta_j}{2}\Big). \tag{38}$$
When $k = N + 1$, according to (30), we obtain
$$\hat{q}_{e_{N+1}} = Ad_{\hat{q}^*_{d_{N(N+1)}}} \hat{q}_{e_N} \circ \hat{q}_{e_{(N+1)'(N+1)}}. \tag{39}$$
According to Lemma A.1, we obtain
$$\begin{aligned} |\ln \hat{q}_{e_{N+1}}| \leq& |\ln \hat{q}_{e_N}| + |\ln \hat{q}_{e_{(N+1)'(N+1)}}| \\ &+ 2\epsilon|\boldsymbol{p}^b_{d_{N(N+1)}}| \sin \frac{|\boldsymbol{\theta}_{e_N}|}{2}. \end{aligned}$$
Applying (38), it follows that
$$\begin{aligned} |\ln \hat{q}_{e_{N+1}}| \leq& \Theta_N + \epsilon\Big(\sum_{i=1}^{N} |\boldsymbol{p}^b_{e_{i'i}}| + 2\sum_{j=1}^{N-1} |\boldsymbol{p}^b_{d_{j(j+1)}}| \sin \frac{\Theta_j}{2}\Big) \\ &+ |\ln \hat{q}_{e_{(N+1)'(N+1)}}| + 2\epsilon|\boldsymbol{p}^b_{d_{N(N+1)}}| \sin \frac{|\boldsymbol{\theta}_{e_N}|}{2}. \end{aligned}$$
Note that $|\boldsymbol{\theta}_{e_N}| \leq \Theta_N$. Then, when $\Theta_N \leq \pi$, we have
$$\sin \frac{|\boldsymbol{\theta}_{e_N}|}{2} \leq \sin \frac{\Theta_N}{2}. \tag{40}$$
Using (40) and noting that $|\ln \hat{q}_{e_{(N+1)'(N+1)}}| = |\boldsymbol{\theta}_{e_{(N+1)'(N+1)}}| + |\boldsymbol{p}^b_{e_{(N+1)'(N+1)}}|$, we obtain
$$\begin{aligned} |\ln \hat{q}_{e_{N+1}}| \leq& \Theta_{N+1} \\ &+ \epsilon\Big(\sum_{i=1}^{N+1} |\boldsymbol{p}^b_{e_{i'i}}| + 2\sum_{j=1}^{N} |\boldsymbol{p}^b_{d_{j(j+1)}}| \sin \frac{\Theta_j}{2}\Big). \end{aligned}$$
Thus, Lemma 1 also holds for $k = N + 1$.

Consequently, by induction, the conclusion follows. □

APPENDIX B
PROOF OF THEOREM 1

Let us denote

$$\xi^b_{j'j} = \xi^b_i - Ad_{\hat{q}^*_{j'j}}\xi^b_j = \xi^b_{j'} - Ad_{\hat{q}^*_{j'j}}\xi^b_j. \tag{41}$$

After some algebraic operations (for details refer to [30]), another form of $\xi^b_{j'j}$ in (41) can be obtained as follows:

$$\xi^b_{j'j} = \omega_{e_{j'j}} + \epsilon(\dot{p}_{e_{j'j}} + \omega_{e_{j'j}} \times p^b_{e_{j'j}}) \tag{42}$$

where $\omega_{e_{j'j}} = \dot{\theta}_{e_{j'j}}$.

We assume that $\hat{k}_j = k_{rj} + \epsilon k_{dj}$ in (25) is a dual number instead of a dual vector for simplicity of analysis. When $\hat{k}_j$ is a dual vector, the same conclusion can be obtained.

Using $\ln \hat{q}_{e_{j'j}} = \frac{1}{2}(\theta_{e_{j'j}} + \epsilon p^b_{e_{j'j}})$, control law (25) can be rewritten as

$$\xi^b_{j'j} = -2\hat{k}_j \cdot \ln \hat{q}_{e_{j'j}} = -k_{rj}\theta_{e_{j'j}} - k_{dj}p^b_{e_{j'j}}. \tag{43}$$

Comparing (42) and (43), it is obtained that

$$\boldsymbol{\omega}_{e_{j'j}} = -k_r\boldsymbol{\theta}_{e_{j'j}} \tag{44}$$

$$\dot{\boldsymbol{p}}^b_{e_{j'j}} + \boldsymbol{\omega}_{e_{j'j}} \times \boldsymbol{p}^b_{e_{j'j}} = -k_d\boldsymbol{p}^b_{e_{j'j}}. \tag{45}$$

Then, we consider the following Lyapunov function candidate:

$$V = \alpha\|\boldsymbol{\theta}_{e_{j'j}}\|^2 + \beta\|\boldsymbol{p}^b_{e_{j'j}}\|^2 \tag{46}$$

where $\|\cdot\|^2$ is the standard two-norm, and $\alpha, \beta > 0$ are scalars. It is seen that V is positive definite and radially unbounded.

Differentiating (46) and then using (44) and (45) yields

$$\begin{aligned}\dot{V} =& 2\alpha\boldsymbol{\theta}^T_{e_{j'j}}\dot{\boldsymbol{\theta}}_{e_{j'j}} + 2\beta\boldsymbol{p}^{b\,T}_{e_{j'j}}\dot{\boldsymbol{p}}^b_{e_{j'j}} \\ =& -2\alpha k_r\boldsymbol{\theta}^T_{e_{j'j}}\boldsymbol{\theta}_{e_{j'j}} - 2\beta\boldsymbol{p}^{b\,T}_{e_{j'j}}(k_d\boldsymbol{p}^b_{e_{j'j}} + \boldsymbol{\omega}_{e_{j'j}} \times \boldsymbol{p}^b_{e_{j'j}}) \\ =& -2(k_r\alpha\boldsymbol{\theta}^T_{e_{j'j}}\boldsymbol{\theta}_{e_{j'j}} + k_d\beta\boldsymbol{p}^{b\,T}_{e_{j'j}}\boldsymbol{p}^b_{e_{j'j}})\end{aligned}$$

which is negative definite.

Therefore, control law (25) causes $|\boldsymbol{\theta}_{e_{j'j}}|$ and $|\boldsymbol{p}^b_{e_{j'j}}|$ asymptotically to converge to 0. That means, for any $\delta' = \delta'_r + \epsilon\delta'_d$, there exists T_j for rigid body $0 < j \le k$ in the path $(0, \ldots, k)$ such that when $t > T_j$

$$|\ln \hat{q}_{e_{j'j}}| = |\boldsymbol{\theta}_{e_{j'j}}| + \epsilon|\boldsymbol{p}^b_{e_{j'j}}| < \delta' = \delta'_r + \epsilon\delta'_d. \tag{47}$$

Denote $p_{d\max} = \max\{|\boldsymbol{p}^b_{d_{j(j+1)}}|, j = 1, \ldots, k-1\}$ in (31). For any $\delta = \delta_r + \epsilon\delta_d > 0$, let δ' in (47) satisfy $0 < \delta'_r < \min\{\frac{1}{k}\delta_r, \frac{2\delta_d}{k(k-1)p_{d\max}}\}$, and let $< \delta'_d < \frac{1}{k}\delta_d - \frac{k-1}{2}p_{d\max}\delta'_r$.

Let $T = \max\{T_i, i = 1, \ldots, k\}$. Substituting (47) into (31), and noticing $0 < \sin\alpha < \alpha$, when $t > T$, we have

$$\begin{aligned}|\ln \hat{q}_{e_k}| <& k\delta'_r + \epsilon(k\delta'_d + \sum_{j=1}^{k-1}|\boldsymbol{p}^b_{d_{j(j+1)}}|\sum_{i=1}^{j}|\boldsymbol{\theta}_{e_{i'i}}| \\ <& k\delta'_r + \epsilon(k\delta'_d + \sum_{j=1}^{k-1}jp_{d\max}\delta'_r) \\ <& \delta_r + \epsilon\delta_d = \delta.\end{aligned}$$

Thus, when $t \to \infty$, $|\ln \hat{q}_{e_k}| \to 0 + \epsilon 0$, which is equivalent to the conclusion in the theorem.

APPENDIX C
PROOF OF THEOREM 2

For any pair of rigid bodies i and j in the overall system, the left-invariant error can be expressed as $\hat{q}_{e_{ij}} = \hat{q}^*_{d_{ij}} \circ \hat{q}_{ij}$. Using (32) yields $\hat{q}_{e_{ij}} = \hat{q}_{e_j} \circ Ad_{\hat{q}^*_{ij}}\hat{q}^*_{e_i}$. From Lemma A.1 and noticing that $\sin\frac{|\boldsymbol{\theta}_{e_i}|}{2} \le \frac{|\boldsymbol{\theta}_{e_i}|}{2}$, we obtain

$$\begin{aligned}|\ln \hat{q}_{e_{ij}}| \le& |\ln \hat{q}_{e_j}| + |\ln \hat{q}^*_{e_i}| + 2\epsilon|\boldsymbol{p}^b_{ij}|\sin\frac{|\boldsymbol{\theta}_{e_i}|}{2} \\ \le& |\boldsymbol{\theta}_{e_j}| + |\boldsymbol{\theta}_{e_i}| + \epsilon(|\boldsymbol{p}^b_{e_j}| + |\boldsymbol{p}^b_{e_i}| + |\boldsymbol{p}^b_{ij}||\theta_{e_i}|)\end{aligned} \tag{48}$$

where $\theta_{e_i} = 2\ln q_{e_i}$, and $\theta_{e_j} = 2\ln q_{e_j}$.

For an arbitrary $\delta = \delta_r + \epsilon\delta_d > 0$, we can choose $\delta' = \delta'_r + \epsilon\delta'_d$ with $0 < \delta'_r < \min\{\frac{1}{2}\delta_r, \frac{\delta_d}{|\boldsymbol{p}^b_{ij}|}\}$ and $0 < \delta'_d < \frac{1}{2}\delta_d - \frac{1}{2}|\boldsymbol{p}^b_{ij}|\delta'_r$. Note that in the dual quaternion weighted tree, rigid bodies i and j have the same lead (rigid body 0). According to Theorem 1, there exists T_i such that for $t > T_i$, $|\boldsymbol{\theta}_{e_i}| < \delta'_r$ and $|\boldsymbol{p}_{e_i}| < \delta'_d$, and there exists T_j such that for $t > T_j$, $|\boldsymbol{\theta}_{e_j}| < \delta'_r$ and $|\boldsymbol{p}_{e_j}| < \delta'_d$.

We choose $T = \max\{T_i, T_j\}$. In view of (48), when $t > T$, one obtains $|\ln \hat{q}_{e_{ij}}| < 2\delta'_r + \epsilon(2\delta'_d + |\boldsymbol{p}^b_{ij}|\delta'_r) < \delta_r + \epsilon\delta_d = \delta$, which means that when $t \to \infty$, $|\ln \hat{q}_{e_{ij}}| \to 0 + \epsilon 0$. Therefore, the conclusion follows.

REFERENCES

[1] M. A. Lewis and K.-H. Tan, "High precision formation control of mobile robots using virtual structures," *Autonomous Robots*, vol. 4, no. 4, pp. 387–403, 1997.

[2] W. Ren and R. W. Beard, "Decentralized scheme for spacecraft formation flying via the virtual structure approach," *J. Guidance, Control, Dyn.*, vol. 27, no. 1, pp. 73–82, 2004.

[3] A. Jadbabaie, J. Lin, and A. S. Morse, "Coordination of groups of mobile autonomous agents using nearest neighbor rules," *IEEE Trans. Autom. Control*, vol. 48, no. 6, pp. 988–1001, Jun. 2003.

[4] R. Sepulchre, D. A. Paley, and N. E. Leonard, "Stabilization of planar collective motion: All-to-all communication," *IEEE Trans. Autom. Control*, vol. 52, no. 5, pp. 811–824, May 2007.

[5] Z. Lin, B. Francis, and M. Maggiore, "Necessary and sufficient graphical conditions for formation control of unicycles," *IEEE Trans. Autom. Control*, vol. 50, no. 1, pp. 121–127, Jan. 2005.

[6] B. D. Anderson, C. Yu, B. Fidan, and J. M. Hendrickx, "Rigid graph control architecture for autonomous formation," *IEEE Control Syst. Mag.*, vol. 28, no. 6, pp. 48–63, Dec. 2008.

[7] H. Wong, H. Pan, and V. Kapila, "Output feedback control for spacecraft formation flying with coupled translation and attitude dynamics," in *Proc. Amer. Control Conf.*, Portland, OR, 2005, pp. 2419–2426.

[8] R. Schlanbusch and P. J. Nicklasson, "Synchronization of target tracking cascadeded leader-follower spacecraft formation," in *Advances in Spacecraft Technologies*, J. Hall, Ed. Rijeka, Croatia: InTech, 2011, pp. 563–584.

[9] Y. Girdhar, A. Xu, B. B. Dey, M. Meghjani, F. Shkurti, I. Rekleitis, and G. Dudek, "Mare: Marine autonomous robotic explorer," in *Proc. IEEE/RSJ Int. Conf. Intell. Robots Syst.*, San Francisco, CA, 2011, pp. 5048–5053.

[10] R. Oung and R. D'Andrea, "The distribute flight array," *Mechatronics*, vol. 21, no. 5, pp. 908–917, 2011.

[11] N. Michael, J. Fink, and V. Kumar, "Cooperative manipulation and transportation with aerial robots," *Auton. Robot*, vol. 30, no. 1, pp. 73–86, 2011.

[12] M. Muller, S. Lupashin, and R. D'Andrea, "Quadrocopter ball juggling," in *Proc. IEEE/RSJ Int. Conf. Intell. Robots Syst.*, San Francisco, CA, 2011, pp. 5113–5120.

[13] R. Featherstone, *Rigid Body Dynamics Algorithm*. New York: Springer-Verlag, 2008.

[14] R. W. Beard, J. Lawton, and F. Y. Hadaegh, "A coordination architecture for spacecraft formation control," *IEEE Trans. Control Syst. Technol.*, vol. 9, no. 6, pp. 777–790, Nov. 2001.

[15] Y. Igarashi, T. Hatanaka, M. Fujita, and M. W. Spong, "Passivity-based attitude synchronization in $SE(3)$," *IEEE Trans. Control Syst. Technol.*, vol. 17, no. 5, pp. 1119–1134, Sep. 2009.
[16] C. Belta and V. Kumar, "Abstraction and control for group of robots," *IEEE Trans. Robot.*, vol. 20, no. 5, pp. 865–875, Oct. 2004.
[17] N. Michael and V. Kumar, "Planning and control of ensembles of robots with nonholonomic constraints," *Int. J. Robot. Res.*, vol. 28, no. 8, pp. 962–975, 2009.
[18] H.-L. Pham, V. Perdereau, B. V. Adorno, and P. Fraisse, "Position and orientation control of robot manipulators using dual quaternion feedback," in *Proc. IEEE/RSJ Int. Conf. Intell. Robots Syst.*, Taipei, Taiwan, 2010, pp. 658–663.
[19] J. Funda, R. Taylor, and R. P. Paul, "On homogeneous transformations, quaternions, and computational efficiency," *IEEE Trans. Robot. Autom.*, vol. 6, no. 3, pp. 382–388, Jun. 1990.
[20] N. Aspragathos and J. Dimitros, "A comparative study of three methods for robot kinematics," *IEEE Trans. Syst., Man, Cybern. B, Cybern.*, vol. 28, no. 2, pp. 135–145, Apr. 1998.
[21] R. M. Murray, Z. Li, and S. S. Sastry, *A Mathematical Introduction to Robotic Manipulation*. Boca Raton, FL: CRC, 1994.
[22] Y. X. Wu, X. P. Hu, D. W. Hu, and J. X. Lian, "Strapdown inertial navigation system algorithms based on dual quaternions," *IEEE Trans. Aerosp. Electron. Syst.*, vol. 41, no. 1, pp. 110–132, Jan. 2005.
[23] M.-J. Kim and M.-S. Kim, "A compact differential formula for the first derivative of a unit quaternion curve," *J. Vis. Comput. Animation*, vol. 7, no. 1, pp. 43–57, 1996.
[24] D. Han, Q. Wei, Z. Li, and W. Sun, "Control of oriented mechanical systems: A method based on dual quaternion," in *Proc. 17th World Congr. Int. Fed. Autom. Control*, Seoul, Korea, 2008, pp. 3836–3841.
[25] M. J. V. Nieuwstadt and R. M. Murray, "Real-time trajectory generation for differentially flat systems," *Int. J. Robust Nonlinear Control*, vol. 8, no. 11, pp. 995–1020, 1998.
[26] D. Mellinger and V. Kumar, "Minimum snap trajectory generation and control for quadrotors," in *Proc. IEEE Int. Conf. Robot. Autom.*, Shanghai, China, 2011, pp. 2520–2525.
[27] H. G. Tanner, G. J. Pappas, and V. Kumar, "Leader-to-formation stability," *IEEE Trans. Robot. Autom.*, vol. 20, no. 3, pp. 443–455, Jun. 2004.
[28] D. Han, Q. Wei, and Z. Li, "Kinematic control of free rigid bodies using dual quaternion," *Int. J. Autom. Comput.*, vol. 05, no. 3, pp. 319–324, 2008.
[29] F. Bullo and R. Murray, "Proportional derivative (PD) control on the Euclidean group," in *Proc. Eur. Control Conf.*, Rome, Italy, 1995, pp. 1091–1097.
[30] X. Wang and C. Yu, "Unit-dual-quaternion-based PID control scheme for rigid-body transformation," in *Proc. 18th World Congr. Int. Fed. Autom. Control*, Milano, Italy, 2011, pp. 9296–9301.
[31] X. Wang and C. Yu, "Feedback linearization regulator with coupled attitude and translation dynamics based on unit dual quaternion," in *Proc. IEEE Int. Symp. Intell. Control*, Yokohoma, Japan, 2010, pp. 2380–2384.

Grasp Input Optimization Taking Contact Position and Object Information Uncertainties into Consideration

Papat Fungtammasan and Tetsuyou Watanabe

***Abstract*—This paper presents a novel approach for grasp optimization considering contact position and object information uncertainties. In practice, it is hard to grasp an object at the designated or planned contact positions, as errors in measurement, estimation, and control usually exist. Therefore, we first formulate the influences of contact uncertainties on joint torques, contact wrenches, and frictional condition. We then include external wrench uncertainties in the required external wrenches set. Based on this formulation, we define the linear grasp optimization problem for two kinds of frictional contact models—frictional point contact and soft finger contact—so that we can successfully grasp an object even if deviations in contact point, object weight, and center of mass occur. The validity of our approach is shown by means of numerical examples and the result of experiments.**

***Index Terms*—Computer and information processing, computer interfaces, grasping, haptic interfaces.**

I. Introduction

Grasping plays an important part in the area of robotics, especially in industrial and household robotics. Many researchers have tried to develop methods to overcome the challenges currently associated with this functionality. However, due to the complexity of the challenges, most of the grasping methods developed so far are for use only in well-defined situations [1]–[5]. For example, in situations where the robot can grasp the target object precisely at the designated positions, the center of mass (CM) can be accurately estimated, and the object is a rigid body.

In practical situations, these assumptions are virtually impossible. For various reasons, differences between the planned (or estimated) and actual values always occur (e.g., measurement, control, and modeling errors). A controller can be used to compensate for these errors, but there is no guarantee that the grasping action will be successful. Several researchers are presently tackling this problem and have proposed various methods to deal with uncertainty in grasping. Chaeah *et al.* [5] represented all the uncertainties in terms of Jacobian uncertainty and proposed an adaptive proportional derivative controller to deal with the problem. Schlegl and Buss [6] proposed hybrid closed-loop control to deal with errors due to control and measurement. Bone and Du [7] presented a new metric that can measure the sensitivity of grasp to contact uncertainty. Zheng and Qian [8] derived the conditions for force closure grasps under contact uncertainty based on the analysis of object motions for force closure. Christopoulos and Schrater [9] created an algorithm to find contact positions to grasp 2-D objects with two contact points under contact uncertainty. Glover *et al.* [10] proposed an algorithm to generate probabilistic models of object geometry. Berenson *et al.* [11] described how to use task space regions to deal

Manuscript received November 3, 2011; revised February 14, 2012; accepted April 24, 2012. Date of publication June 18, 2012; date of current version September 28, 2012. This paper was recommended for publication by Associate Editor C. C. Cheah and Editor J.-P. Laumond upon evaluation of the reviewers' comments. This work was supported by Grants-in-Aid for Scientific Research under Grant 20760162.

The authors are with the College of Science and Engineering, Kanazawa University, Kanazawa 920-1192, Japan (e-mail: papatffuture@gmail.com; te-watanabe@ieee.org).

Color versions of one or more of the figures in this paper are available online at http://ieeexplore.ieee.org.

Digital Object Identifier 10.1109/TRO.2012.2197310